Journal of Applied Physics

Magnetoresistance peaks in the neighborhood of coercivity in magneto-optical recording media

Cite as: Journal of Applied Physics **72**, 1528 (1992); https://doi.org/10.1063/1.351721
Submitted: 09 October 1991 . Accepted: 27 April 1992 . Published Online: 17 August 1998

Roger A. Hajjar, and M. Mansuripur

Magnetoresistance peaks in the neighborhood of coercivity in magneto-optical recording media

Roger A. Hajjar and M. Mansuripur
Optical Sciences Center, University of Arizona, Tucson, Arizona 85721

(Received 9 October 1991; accepted for publication 27 April 1992)

Perpendicular magnetoresistance data performed on magneto-optical samples with uniaxial magnetic anisotropy (perpendicular to the film plane) show a change of the resistance $\Delta R/R$ when the applied field reaches the coercive field. The various mechanisms that can lead to this phenomenon are investigated based on different magneto-optical films. In particular, the interaction of magnetic domains and domain walls with the electric current is interesting. Separating the two effects is important to understanding of the various galvanomagnetic and magnetic processes in these films. Three different mechanisms are considered in order to explain the data: The first mechanism is associated with the Hall effect, the second mechanism involves the anisotropic resistivity, and the third mechanism is related to the *s-d* scattering effect. Some of the experimental results are explained by modeling the current and electric-field distribution in these films. In the simulations the film is modeled by a two- or three-dimensional lattice with each branch in the lattice having its own resistivity tensor in order to simulate magnetic domains and domain walls in the film.

I. INTRODUCTION

Previous perpendicular magnetoresistance (MR) measurements performed on magneto-optical (MO) samples such as GdCo,[1] TbFe,[2] TbFeCo,[3] and Co/Pt and Co/Pd (Refs. 2 and 4) films show a change of the resistance $\Delta R/R$ when the applied field reaches the coercive field. In this magnetoresistance geometry, a magnetic field is applied normal to the plane of the film and the resistance is measured across point contacts A and C ($\Delta R_{AC}/R$) or B and D ($\Delta R_{BD}/R$) as illustrated in Fig. 1. The terminology $\Delta R/R$ will be used when $\Delta R_{AC}/R$ equals $\Delta R_{BD}/R$. The Hall effect is also monitored simultaneously with the magnetoresistance measurement across the other pair of contact points. The peak is generally centered around the coercive field and can be due to several mechanisms: The first mechanism is associated with the Hall effect, the second involves the anisotropic resistivity, and the third mechanism is related to the *s-d* scattering effect. In order to study all three effects, we consider three samples with different Hall angle ϕ_h ($=\rho_h/\rho$) and domain configuration in the demagnetized state. The first sample is a Co/Pt film with a moderate ϕ_h and a random domain configuration. The second sample is a TbFeCo film with a high ϕ_h and an asymmetric domain pattern, and the third sample is a Co/Pd film with a low ϕ_h and a large number of domains (i.e., below the resolution limit of an optical polarization microscope). Table I summarizes the galvanomagnetic and magneto-optical properties of the samples with their respective normalized Hall hysteresis loops (see Fig. 2).

II. *s-d* SCATTERING EFFECT

Let us consider first the *s-d* scattering effect. Figure 3(a) displays the magnetoresistance measurement $\Delta R/R$ for a film composed of ten bilayers of Co(4 Å)/Pt(13 Å) deposited by Kr sputtering (7 mTorr) on a 1000 Å ZnO underlayer. The sample is initially in its saturated state with the magnetization vector in the z direction. As the field increases in a direction parallel to the magnetization, a decrease in the resistance is observed and has its origin in the *s-d* scattering phenomenon as interpreted by Mott.[5] The *s-d* scattering effect, also known as the two-current model, has been extensively studied in the literature and widely applied for transition ferromagnets.[6] In simple terms it is related to the difference between *d*-up and *d*-down densities of states at the Fermi level. This difference will cause the *s-d* scattering rates to be different for spin-up and spin-down conduction electrons. Therefore, as the spontaneous magnetization increases due to a parallel magnetic field, the population of spin-up electrons in the *d* band increases which reduces the probability of scattering for the spin-up conduction electrons, thus resulting in a lower resistance. When the field is antiparallel to the magnetization (i.e., before the coercivity is reached), the population of spin-up electrons in the *d* band is reduced creating vacancies for the spin-up conduction electrons to scatter into, resulting in a higher resistance. At the coercive point, the sample is in its demagnetized state and shows no apparent increase of the resistance. This is usually not the case in other MO films including other Co/Pt samples, where a pronounced change of resistance is observed at $H = H_c$; there the phenomenon might be a consequence of the Hall effect or the anisotropic resistivity effect as we shall see in the following section.

III. HALL EFFECT AND ANISOTROPIC RESISTIVITY

Next we consider the magnetoresistance mechanisms due to the Hall effect and anisotropic resistivity. We combine the two effects at first since they are intimately related in the sense that one effect originates from the domains while the other originates from the domain walls covering the film. Depending on whether the MO film is of the nucleation type or the domain-wall motion type, one mech-

 0021-8979/92/161528-11$04.00

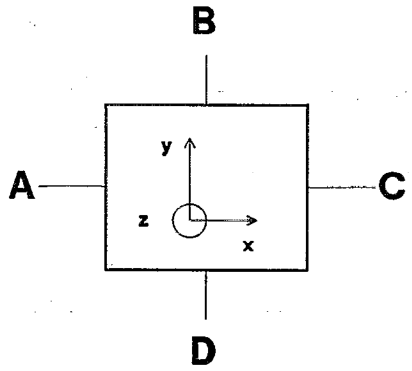

FIG. 1. Magnetoresistance geometry with point contacts A, B, C, and D.

anism might dominate the other. In order to give a general description of the two effects let us consider a MO sample in its demagnetized state. We represent the domains and domain walls by their own resistivity tensor which is directly related to the local state of magnetization. In a simple-minded argument, the difference between an up and down magnetized domain is a reversal of the sign of the Hall resistivity ρ_h assuming that the resistivity ρ is equal to ρ_z in either case. Therefore, the resistivity tensor for an up ($\uparrow$) or down ($\downarrow$) magnetized domain can be represented as

$$\rho_{\uparrow(\downarrow)}=\begin{pmatrix} \rho_z & \mp\rho_h \\ \pm\rho_h & \rho_z \end{pmatrix}. \tag{1}$$

This abrupt reversal of the Hall resistivity causes a nonuniform current distribution at the wall. There the Lorentz force is no longer balanced by the Hall voltage, and the conduction electrons are deflected causing nonuniform current density near the wall.[7] This change in the current distribution creates an internal Hall voltage across the current leads causing a change in the apparent resistance of the sample. We will simulate this Hall-effect mechanism with different domain configurations and different magnetoresistance geometries.

In addition to the Hall effect, the domain walls themselves can induce scattering of the current. At the domain walls the Hall resistivity can vanish since the magnetization lies in the plane of the film. Now the resistivity tensor

TABLE I. Magnetic and galvanomagnetic properties of the samples studied. The values of θ_k, H_c, ρ_h, and ρ are at room temperature. The corresponding normalized hysteresis loops for the three samples are displayed in Figs. 2(a), 2(b), and 2(c).

Sample	θ_k (deg)	H_c (kOe)	Normalized Hall hysteresis loop	ρ_h ($\mu\Omega$ cm)	ρ ($\mu\Omega$ cm)
Co(0.4 nm)/ Pt(1.3 nm) 17 nm	0.18	2.4	Fig. 2(a)	0.51	50
Co(0.2 nm)/ Pd(0.9 nm) 27.5 nm	0.15	2.4	Fig. 2(b)	0.018	68
$Tb_{16}Fe_{77}Co_7$ 50 nm	0.74	2.2	Fig. 2(c)	5.65	183

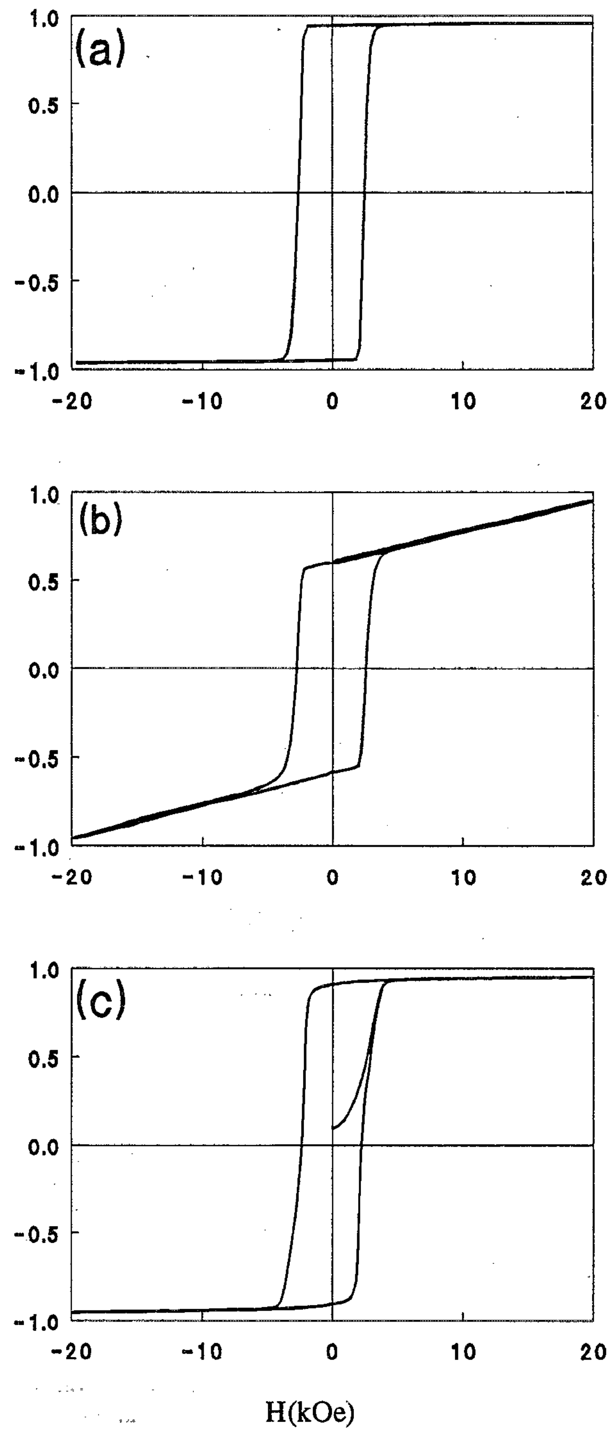

FIG. 2. Normalized Hall hysteresis loops for the three samples as indicated in Table I.

contains only the diagonal resistivity terms ρ_x and ρ_y associated with the direction of the magnetization in the plane of the film,

$$\rho_{\text{wall}}=\begin{pmatrix} \rho_x & 0 \\ 0 & \rho_y \end{pmatrix}. \tag{2}$$

The effective resistivity ρ seen by the current density $\mathbf{J}$

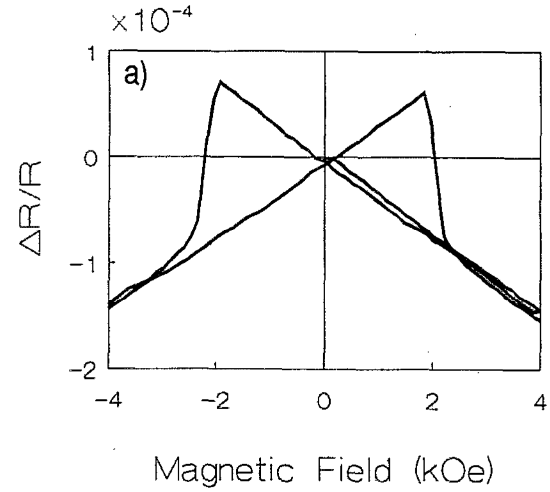

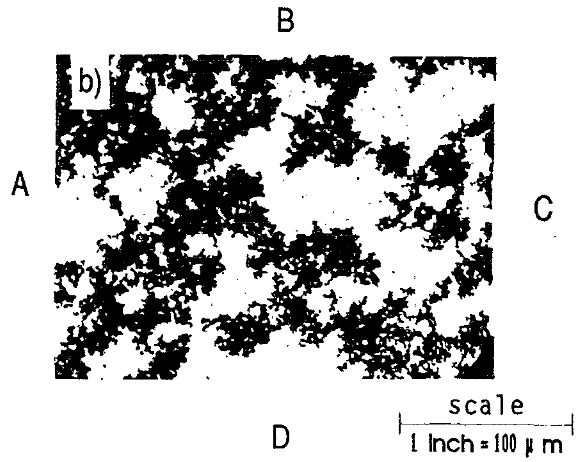

FIG. 3. (a) Perpendicular magnetoresistance measurement performed on a Co/Pt sample. Note no apparent change of the magnetoresistance at H_c. The dominant effect is due to the *s-d* scattering. (b) A polarization microscope photograph of the Co/Pt sample showing few random domains and domain walls distributed in the sample.

depends on the angle α between **J** and the direction of the magnetization in the plane of the sample. From Ohm's law we have

$$\rho=\rho_y+(\rho_x-\rho_y)\cos^2\alpha, \tag{3}$$

where ρ_x and ρ_y are the resistivity values when $\alpha=0°$ or $\alpha=90°$, respectively. Since ρ_y and ρ_z correspond to the magnetization direction being perpendicular to the current direction we can assume $\rho_y = \rho_z$. We define $\Delta\rho = \rho_x - \rho_z$ to be the anisotropic resistivity of MO films. In all the MO films measured at room temperature we found $\Delta\rho>0$ from the longitudinal magnetoresistance[2] measurement. The anisotropic resistivity has been discussed initially by Smit[8] and is due to the increased scattering of the conduction electrons travelling parallel to the magnetization and is mediated by the spin-orbit interaction.

Based on this argument we expect a current flowing in a demagnetized MO sample to be affected by either the domains or the domain walls. In the following subsection we will show both experimentally and theoretically the effects introduced by the magnetic domains due to the Hall effect.

A. Hall effect

Several authors have treated the effect of the Hall voltage on the magnetoresistance.[3,7,9,10] When an electric current flows in a magnetic specimen it is subject to a Lorentz force which gives rise to a Hall voltage balancing the Lorentz force. This Hall voltage depends on the distribution of current and magnetization inside the film and can exist anywhere in the sample. In multiple domain samples the current has been found to zigzag creating the appearance of an excess resistance on the current leads.[1,2] With many equal-width stripe domains the magnetoresistance is maximum and is related to both the Hall angle and the orientation of the wall with respect to the current. If $\beta=|\tan(\phi_h)|\ll 1$,

$$\Delta\rho/\rho=\beta^2\sin^2\psi, \tag{4}$$

where ψ is the angle between the wall and the current.[10] This expression is not valid when the domains are not stripes, or when the current takes a nonuniform path in the film. In general, jagged and irregular domain patterns are most likely to occur in MO films and a uniform current distribution throughout the film is difficult to achieve experimentally.

We consider a $Tb_{16.1}Fe_{77}Co_{6.9}$ 500-Å-thick sample to illustrate the effect of the Hall voltage on the magnetoresistance. The solid trace in Fig. 4(a) is a measurement of $\Delta R_{AC}/R$ with the sample initially demagnetized (perpendicular geometry). As the field increases the resistance decreases since fewer domains exist in the film. From the argument presented above, the decrease of the resistance can be due to both the decrease in domains and domain walls in the film. In order to verify which effect is the dominant one, we shorted leads B and D and repeated the measurement of $\Delta R_{AC}/R$. The resulting dashed curve is also shown in Fig. 4(a). In this measurement, the Hall current produced by the magnetization in the film is allowed to flow in a direction transverse to the average direction of the electric current. This Hall current will produce a secondary Hall voltage on the current leads, therefore increasing the apparent resistance of the sample. When the Hall current is zero, the sample is in its demagnetized state and its resistance is the same whether or not leads B and D are shorted. There are three field values were the solid and dashed curves meet: the initial state at zero field and at the $\pm$ H_c coercive field. The sample is initially demagnetized by applying an in-plane field and monitoring the Hall voltage across leads B and D. Figure 4(b) is a trace of the Hall voltage as a function of field. We note that after scanning repeatedly the field from its maximum to its minimum value, the Hall voltage is eventually brought to zero, indicating that the sample is in its demagnetized state. At this point the resistance of the sample is

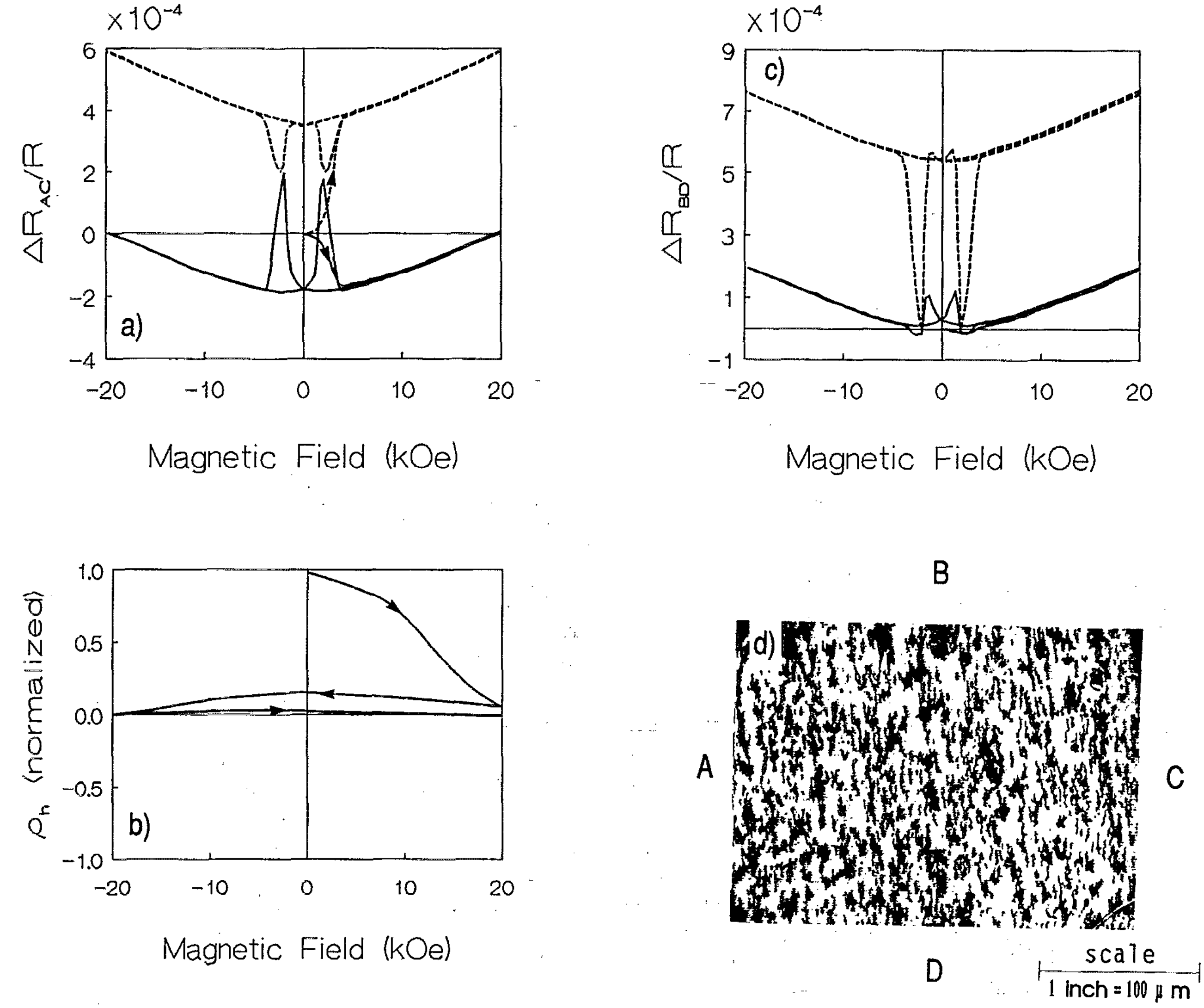

FIG. 4. (a) Magnetoresistance across the AC leads for a TbFeCo sample with (dashed trace) and without (solid trace) the Hall leads shorted. (b) Normalized Hall effect obtained with an in-plane magnetic field. After repeatedly scanning the magnetic field the Hall voltage is eventually brought to zero implying that the sample is in its demagnetized state. (c) Magnetoresistance across the BD leads for a TbFeCo sample with (dashed trace) and without (solid trace) the Hall leads shorted. (d) A polarization microscope photograph showing the orientation of the domains and the relative position of the four-point contacts.

the same whether or not the leads are shorted. The other two values of the field where the sample is also in its demagnetized state correspond to the coercivity points (i.e., where the Hall hysteresis loop crosses zero). At this point the peaks in both traces in Fig. 4(a) meet. Note that the magnetoresistance value at the peaks is different from that in the initial state even though both cases correspond to a demagnetized sample. This implies that the domain-configuration is different in two cases. The fact that the peaks in these two measurements (solid and dashed trace) met may be taken as evidence that the active mechanism here is the Hall effect. For instance if scattering from the domain walls were present the peaks would always be positive, whether or not the Hall leads were shorted.

The same sample has its $\Delta R_{BD}/R$ measured from the saturated state. This measurement is shown in Fig. 4(c). Note the difference of the peaks between Figs. 4(a) and 4(c). This difference is attributed to different domain configuration with respect to the current direction. Figure 4(d) is a polarization microphotograph of the film near the coercive field, showing the orientation of the domains. $\Delta R_{BD}/R$ is along the stripes while $\Delta R_{AC}/R$ is perpendicular to the stripes. Later, using numerical calculations we will show that the results obtained here are in agreement with the Hall-effect mechanism. Finally, note the positive slope observed in Figs. 4(a) and 4(c). The slope occurs after the sample has been saturated and is independent of the Hall effect. This slope has been discussed in the literature[2,3] and may be related to the dispersion of the Terbium moment.

B. Anisotropic resistivity

Perpendicular MR measurements are performed on a Co(2 Å)/Pd(9 Å) 275-Å-thick film sputter deposited on a

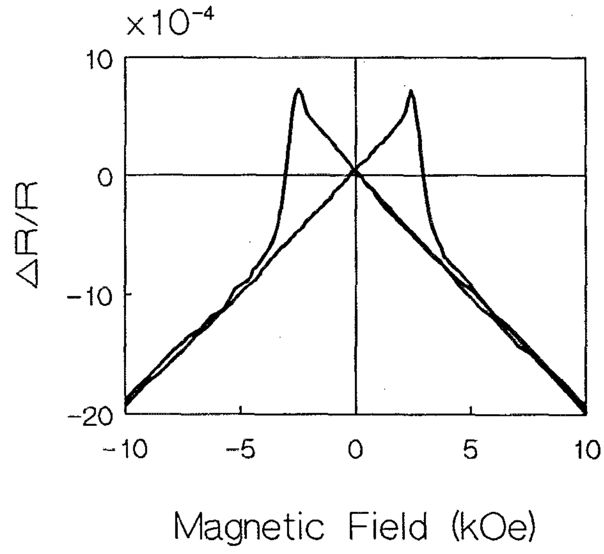

FIG. 5. Magnetoresistance of a Co/Pd sample. Note the peaks obtained near the coercive field. In addition to the *s-d* scattering, the peaks originate from domain-wall scattering.

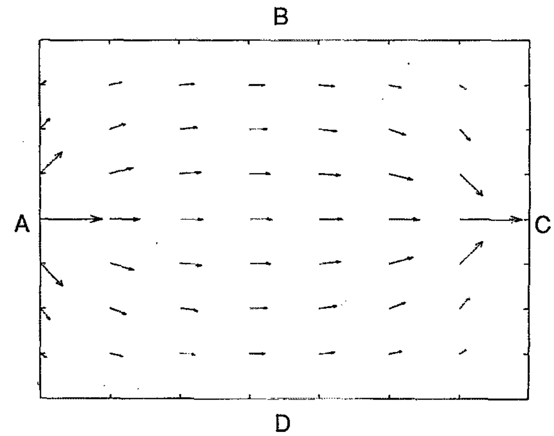

FIG. 6. Simulation of current distribution in a square sample using point contact geometry. The point contacts A, B, C, and D are symmetrically located around the square.

glass substrate at 10 mTorr pressure of krypton gas. For this sample ϕ_h is almost two orders of magnitude less than that in TbFeCo films. Since ϕ_h is low the ordinary Hall effect is clearly present on the Hall loop (see Table I). Even though this sample has a modest Kerr rotation θ_k we could not observe any domains under the optical microscope. This might indicate that the sample is nucleation dominated with domains smaller than the resolution of our microscope ($\simeq 0.5$ μm). The $\Delta R/R$ measurement for this sample is shown in Fig. 5. Besides the *s-d* scattering effect an excess $\Delta R/R$ of about 2×10^{-4} is observed at the coercive field. $\Delta R/R$ measurements performed on other Co/Pt and Co/Pd samples show little or no effect by shorting the Hall leads. We therefore believe that the excess resistance at H_c is due to scattering from the domain walls, and that the Hall-effect mechanism due to the presence of domains in the sample is not at work here. Therefore the height of the peak in this film is a measure of the volume fraction of domain walls covering the sample. The Co/Pt sample discussed earlier (see Fig. 3) did not show any apparent change of the resistance at H_c. For this sample we could observe magnetic domains in the demagnetized state as shown in Fig. 3(b).

IV. SIMULATIONS

A. 2D simulations

In order to study the contribution of the Hall effect to magnetoresistance we use the two-dimensional lattice model described in the Appendix. In the simulations that follow ρ is fixed throughout the sample but ρ_h takes the values of $\pm 0.1\rho$ (the sign depends on the direction of magnetization perpendicular to the sample) and vanishes at the domain wall. The value of the Hall angle ϕ_h is somewhat larger than the one observed experimentally, however our choice is limited by the numerical precision. The results, however, give us the relative increase or decrease of the resistance depending on the domain patterns and help us explain the experimental results.

1. Initial run

Example 1: Figure 6 shows the distribution of the current when $\rho=1$ in the absence of any magnetization ($\rho_h = 0$). A constant current flows through points A and C and the resistance of the film is obtained by dividing the voltage across these two points by the total current. The resistance R_0 obtained is equal to 2.5377.

2. Saturated sample

Example 2: Next we consider the sample to be uniformly magnetized normal to the film plane ($\rho_h = 0.1$). As a result the magnetoresistance of the film $(R_{\rm sat} - R_0)/R_0$ is 1.58×10^{-4}. This increase in resistance is mainly due to the divergence of the current as it enters the film. This is a consequence of the point contact geometry. In the remainder of the simulations $\Delta R/R$ will be computed relative to the saturated state of the film [i.e., $\Delta R/R = (R_{\rm domains} - R_{\rm sat})/R_{\rm sat}$] since this is the quantity we measure in our experiment.

3. Two stripes

Example 3: The sample is now divided equally between an up and down region of magnetization with the wall ($\rho_h = 0$) being perpendicular to the current direction. Figure 7 is obtained by subtracting the current distribution from Fig. 6. The relative increase of resistance from the fully saturated film is 18.52×10^{-4}. Figure 7 shows a current loop centered on the wall. This phenomenon has been studied in the literature[10] and often called a dc "eddy currents." This eddy current causes an increase of the Joule dissipation in the sample which increases its effective resistance. Another way to understand the excess resistance is to consider the current components in the loop that are perpendicular to the direction of the applied cur-

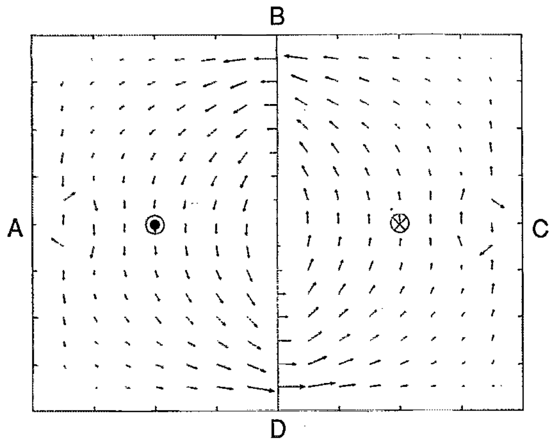

FIG. 7. Resulting current distribution due to a wall perpendicular to the average current direction.

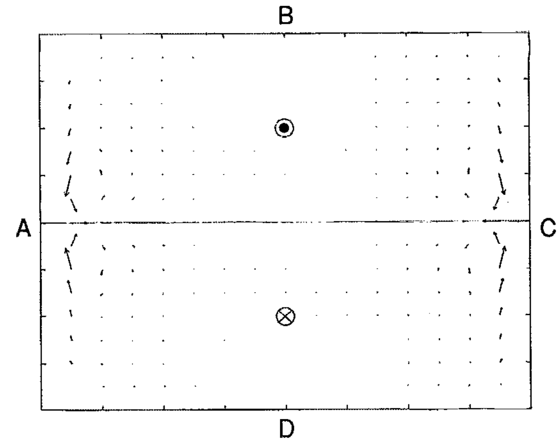

FIG. 9. Resulting current distribution due to a wall parallel to the average current direction.

rent as shown schematically in Fig. 8. These components of current in their interaction with the magnetization of the film will produce a Hall volatge at the leads. This Hall voltage will always add to the resistance of the film as shown in Fig. 8.

Another consequence of the current loop is the generation of a magnetic field perpendicular to the film plane. This field will exert a force on the wall and can, in principle, induce propagation of magnetic domains. This effect is observed when the current density exceeds a threshold value associated with the domain-wall coercivity and has been observed in several "bubble" media such as GdCoMo and GdCoAu.[11,12] We did not consider the domain drag effect in our calculations, since it occurs at relatively high current densities or when the coercivity of the material is much lower than the magneto-optical media.

Example 4: The wall is now oriented parallel to the current direction and the effect on the resistance is found to be minimal. The resulting resistance in this case fell to the value obtained when the film has no magnetization $\rho_h = 0$. Figure 9 shows the calculated current distribution produced by stripe domains parallel to the current.

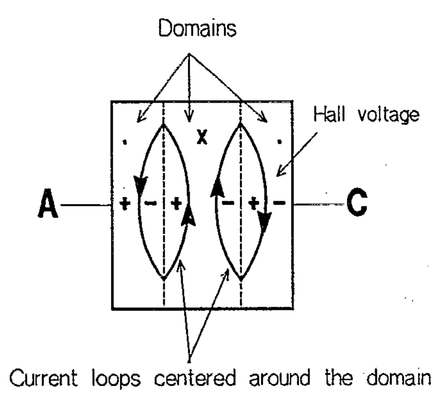

FIG. 8. Hall voltage generated by current loops centered on the walls increasing the apparent resistance of the sample.

4. Multiple stripes

Example 5: The sample now contains multiple stripes separated with domain walls perpendicular to the current direction. In the case of five stripes perpendicular to the average current flow, the current distribution can be decomposed into the initial one of Fig. 6 and that of Fig. 10. There are several current loops centered on the walls. Again the current components perpendicular to the original current direction contribute a voltage through the Hall effect and increase the apparent resistance of the film. This relative increase is 28.36×10^{-4} from the initial saturated state.

Example 6: When the five stripes are parallel to the current leads, an increase of $\Delta R/R = 8.67 \times 10^{-4}$ is observed. This is related to the nonuniform current distribution in the film due to the point contact geometry. Figure 11 shows the current distribution in the film due to the domains in this example.

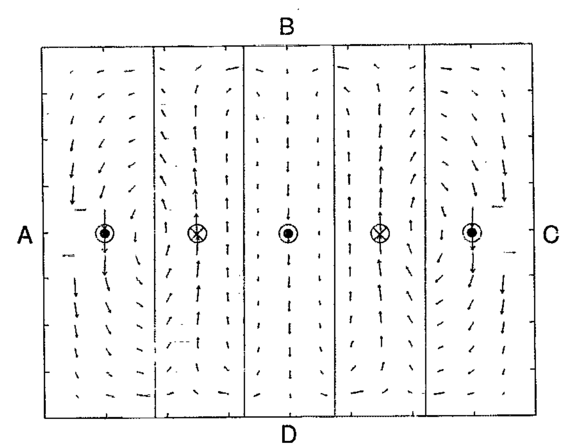

FIG. 10. Resulting current distribution due to five stripes perpendicular to the average current direction.

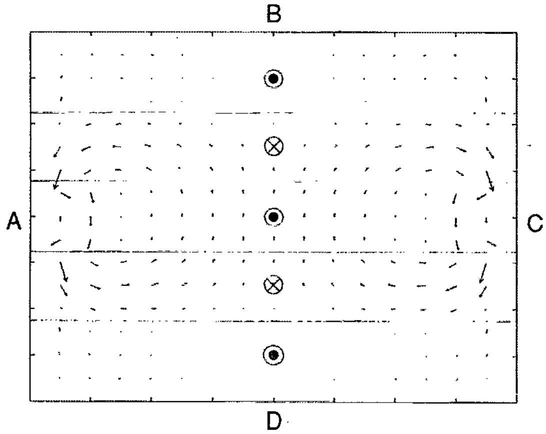

FIG. 11. Resulting current distribution due to five stripes parallel to the average current direction.

5. Quadrants

Example 7: The film is now divided into nine square domains separated by domain walls. The relative change of resistance from the saturated state is -1.18×10^{-4}. This result shows that the Hall effect in nucleation-dominated samples will not affect the resistance severely. This can be explained by the short-range bending of the current lines in one direction due to the spatial distribution of domains in the film. Figure 12 shows the resulting current distribution due to the checkerboard domain configuration.

6. Shorting the Hall leads

We short the leads by connecting point B to point D in the simulations. The resulting calculated relative changes of resistance are summarized in Table II. Note that film's resistance is increased by effectively 15.36×10^{-4} from the saturated state. This increase is due to the generation of an internal Hall voltage across the current leads as explained earlier in the experimental results. The total change of the resistance when the film breaks into domains between the

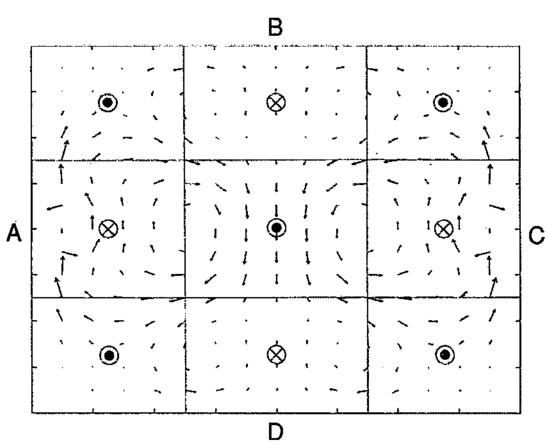

FIG. 12. Resulting current distribution due to a checkerboard domain pattern.

TABLE II. Results of $\Delta R/R$ from the simulations of the Hall-effect mechanism with different domain patterns. Column 2 is obtained by shorting the Hall leads (BD). Note that $\Delta R/R$ in the first two rows correspond to the relative difference between the saturated state ($\rho_h=0.1$) and the nonmagnetized state ($\rho_h=0$), while $\Delta R/R$ in rows 3–9 correspond to the relative difference between the given state and the saturated state.

Magnetization state	$\Delta R/R\times10^{-4}$ (Hall leads not shorted relative to $\rho_h=0$)	$\Delta R/R\times10^{-4}$ (Hall leads shorted relative to $\rho_h=0$)
Up ($\rho_h=0.1$)	1.58	16.95
Down ($\rho_h=-0.1$)	1.58	16.95
	Relative to saturated state	Relative to saturated state
2 ∥ stripes	−1.58	−16.91
2 ⊥ stripes	18.52	3.15
3 ∥ stripes	7.09	−8.26
3 ⊥ stripes	24.82	9.44
5 ∥ stripes	8.67	−5.51
5 ⊥ stripes	28.36	13.77
9 Quadrants	−1.18	−16.52

first and the second column in Table II is a constant equal to the offset produced by shorting the hall leads.

B. 3D simulations

This subsection discusses the magnetoresistance effects observed when we apply in-plane fields. The purpose of this subsection is twofold. First, we explain the contribution of the different mechanisms (Hall effect, *s-d* effect, and anisotropic resistivity) to the results. Second, we discuss the differences between point and bar contacts geometries and their effects on the measurements.

Let us consider, for example, a typical set of in-plane magnetoresistance measurements performed on a Co/Pt sample[2] as shown in Fig. 13. Figures 13(a) and 13(b) show $\Delta R_{AC}/R$ and $\Delta R_{BD}/R$ when the field is applied in the x direction as shown in Fig. 1. $\Delta R_{AC}/R$ corresponds to the longitudinal geometry and $\Delta R_{BD}/R$ corresponds to the transverse geometry. At first, the sample is saturated along the easy axis. Both longitudinal and transverse geometries show the following features: as H increases an initial increase of the resistance is observed followed by a maximum point once the magnetization is brought all the way in the plane of the sample. The maximum change of resistance occurs at the anisotropy field H_k of 12 kOe in this case. Once the magnetization and the field have been aligned, further increase of H causes the resistance to drop in a linear fashion reminiscent of the *s-d* scattering effect discussed earlier. We will address next whether the initial increase of resistance is due to a backlash of the Hall effect or due to the anisotropic resistivity.

1. Hall effect

As a result of forcing the magnetization in the direction of H, and depending on the geometry used, a Hall voltage might develop across the current leads. For instance, in the transverse geometry, we expect a Hall voltage to develop in the z direction across the thickness of the film. We simulated the effect of the Hall mechanism using

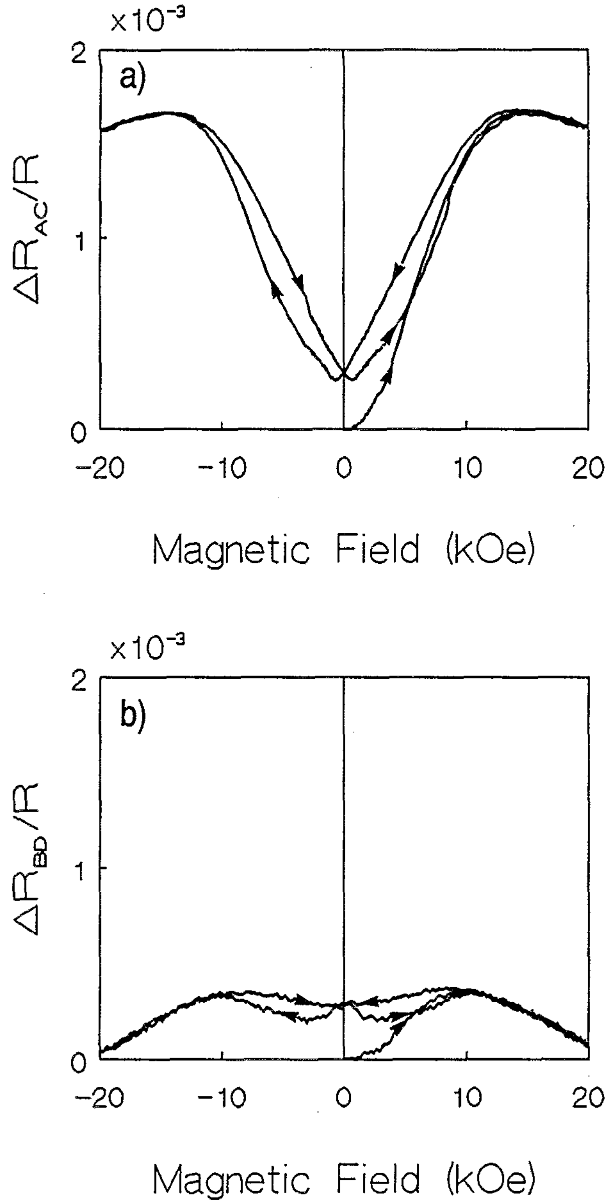

FIG. 13. (a) Longitudinal and (b) transverse magnetoresistance measurements performed on a Co/Pt sample. The sample is initially in its saturated state.

a 3D lattice configuration (see the Appendix) in order to calculate the change of resistance as the magnetization is brought in the plane of the film. The results for both the longitudinal and transverse geometries show equal amount of decrease of the magnetoresistance which is contrary to the increase observed in the data. The total amount of decrease of the resistance (i.e., from saturated to in-plane magnetization) is the same as if the Hall resistivity of the film changed from a finite value to zero independently of the geometry used. This is not surprising, since for thin films, the Hall voltage that develops across the thickness of the film becomes negligible: i.e., the current flowing in the z direction is too small to cause any considerable effect. Since the relative decrease in resistance was contradictory to the change observed in our measurements, we conclude that the dominant mechanism here is the anisotropic resistivity which is discussed below.

2. Anisotropic resistivity

We discuss the effect of the anisotropic resistivity on the in-plane MR measurements given different current orientations (longitudinal and transverse) and different contact geometries (bar and point contact). As the magnetization is brought in the plane of the film along the x direction, the current will interact with an effective resistivity which is a function of the anisotropic resistivity as discussed earlier [see Eq. (3)]. Let us assume a $\Delta\rho = \rho_x - \rho_z = 0.1$ and a $\rho_z = 50\,\mu\Omega$ cm with $\rho_z = \rho_y$.

a. Longitudinal configuration. In the case of point contacts along the x direction, the relative difference of the resistance between an in-plane magnetization along the x axis and a saturated magnetization along the z axis is $\Delta R/R = (R_{\text{in plane}} - R_{\text{saturated}})/R_{\text{saturated}} = 1.3 \times 10^{-3}$. In the case of bar contacts the calculated $\Delta R/R = \Delta\rho/\rho_z = 2 \times 10^{-3}$.This discrepancy of almost 35% is related to current components along the y direction in the case of point contacts.

b. Transverse configuration. In the transverse configuration the current is applied in the y direction and similarly, $\Delta R/R$ corresponds to the relative difference between an in-plane magnetization along the x axis and a saturated magnetization along the z axis. If bar contacts are used, $\Delta R/R = 0$ as expected since we assumed $\rho_z = \rho_y$. However, if point contacts are used, $\Delta R/R = 0.7 \times 10^{-3}$ due to current components along the x direction.

The simulations using point contact geometries are in close agreement with the experimental data as shown in Figs. 13(a) and 13(b).

V. CONCLUSIONS

We investigated three different sources of magnetoresistance in MO films. After examining the experimental and theoretical results we conclude the following.

When the applied field is perpendicular to the sample:

(i) The s-d mechanism can be dominant in cobalt based multilayers such as Co/Pt [Fig. 3(a)] due to the presence of few domain walls and a small Hall angle.

(ii) The magnetoresistance is affected by both the domain walls through the anisotropic resistivity mechanism (Fig. 5) and domains through the Hall-effect mechanism [Figs. 4(a) and 4(c)].

(iii) We observe that the Hall effect generated due to magnetic domains can induce an increase or decrease of the resistance of the sample. This behavior is, of course, strongly related to the current direction with respect to the domain configuration in the sample [Figs. 4(a) and 4(c)].

When the applied field is parallel to the sample:

(i) The Hall-effect mechanism is negligible in the longitudinal and transverse magnetoresistance geometry for Mo films. The dominant contributions in these measurements are from the anisotropic resistivity and the s-d mechanisms.

(ii) In the case of point-contact geometry, the transverse magnetoresistance can be as high as 50% of the longitudinal magnetoresistance due to the eye-shaped current distribution. In the case of longitudinal magnetoresistance a 35% decrease is obtained when using point contacts as opposed to bar contacts which is also a consequence of the current distribution.

ACKNOWLEDGMENTS

The authors are grateful to Dr. P. Carcia of Dupont Central Research and Development and to Dr. C. Brucker of Kodak Research Laboratories for providing the multilayer samples. We wish to thank Dr. T. Yorozu and his group of Optical Storage Research Center for supplying the TbFeCo samples. Thanks are also due to Mr. Bruce Bernacki for taking the polarization microscope photograph and to Te-Ho Wu for assisting in the measurements. R. A. H. would like to acknowledge the support of an IBM fellowship.

APPENDIX: MODELING OF THE CURRENT DENSITY AND ELECTRIC FIELD IN MAGNETIC FILMS

Our approach consists of modeling the film as a square lattice in the two-dimensional (2D) case or into a cubical lattice in the three-dimensional (3D) case, as shown in Fig. 14. The 2D lattice is similar to the 3D one except that in the latter case we can solve for the current in the z direction. As shown in Fig. 14 the film is divided into a mosaic of square tiles with each tile having the dimensions $l\times l\times t$. Here t is the film thickness and l is the length of each tile on the side. There are a total of $n\times n$ nodes covering the sample in the 2D lattice and $n\times n\times 2$ nodes in the 3D case. A more refined geometry would correspond to a hexagonal or higher-order polygonal tiles; however, our intent here is to show the feasibility of the concept with the least-complicated model and to explain the features of the phenomena observed in real films.

Each branch in the lattice is associated with a resistivity ρ_ξ where ξ is the branch direction (i.e., $\xi=x$, y, or z) and an extraordinary Hall resistivity ρ_h. A current density J_ξ flows through each branch and an electric field E_ξ develops across it.

In order to solve for the current distribution in the steady state, the following two electrostatic Maxwells equations apply throughout the lattice:

$$\operatorname{div} \mathbf{J}=0, \tag{A1}$$

$$\operatorname{curl} \mathbf{E}=0. \tag{A2}$$

With the electric field related to the current density by the resistivity tensor,

$$\mathbf{E}=\begin{pmatrix} \rho_x & \mp\rho_h \\ \pm\rho_h & \rho_y \end{pmatrix}\mathbf{J}, \tag{A3}$$

for the 2D lattice. The $\pm$ sign corresponds to an up or down magnetization direction along the z axes. For the 3D lattice the relation between $\mathbf{E}$ and $\mathbf{J}$ is given by

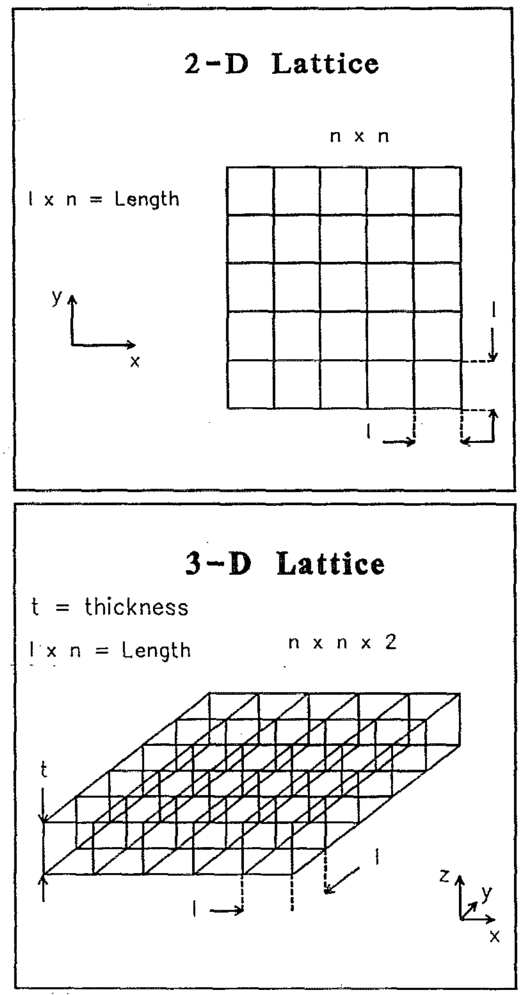

FIG. 14. Modeling of the sample by a 2D and 3D lattice. The 2D lattice consists of $n\times n$ tiles while the 3D lattice consists of $n\times n\times 2$ tiles. Each tile has the dimensions $l\times l\times t$ in the 2D lattice or $l\times l\times t/2$ in the 3D lattice.

$$\mathbf{E}=\begin{pmatrix} \rho_x & -\rho_h\cos\theta & \rho_h\sin\theta\sin\phi \\ \rho_h\cos\theta & \rho_y & \rho_h\sin\theta\cos\phi \\ \rho_h\sin\theta\sin\phi & \rho_h\sin\theta\sin\phi & \rho_z \end{pmatrix}\mathbf{J}. \tag{A4}$$

Here θ and ϕ are the angles that the magnetization vector makes with respect to z and x axes, respectively.

In order to solve for the current distribution, Eqs. (A1) and (A2) and the corresponding relations in Eq. (A3) or Eq. (A4) yield a system of N linear equations expressed in terms of the N current densities in the lattice. Let $\mathbf{J}$ be an $N\times 1$ vector containing all the current densities in the lattice and $\mathbf{J}_{\text{appl}}$ be another $N\times 1$ vector containing the input and output current densities applied to the lattice at specific nodes, then the N equations can be represented in matrix form as

$$\mathbf{AJ}=\mathbf{J}_{\text{appl}}, \tag{A5}$$

where $\mathbf{A}$ is an $N\times N$ matrix containing the coefficients of

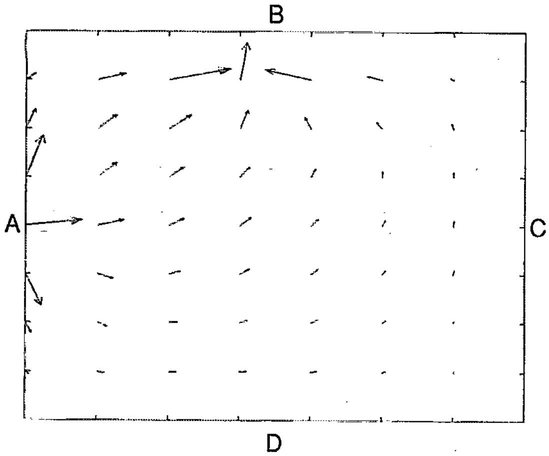

FIG. 15. Application of the Van der Pauw technique consists of applying a current through A and B and measuring the potential drop across C and D. The figure shows an example of a 7×7 lattice mesh.

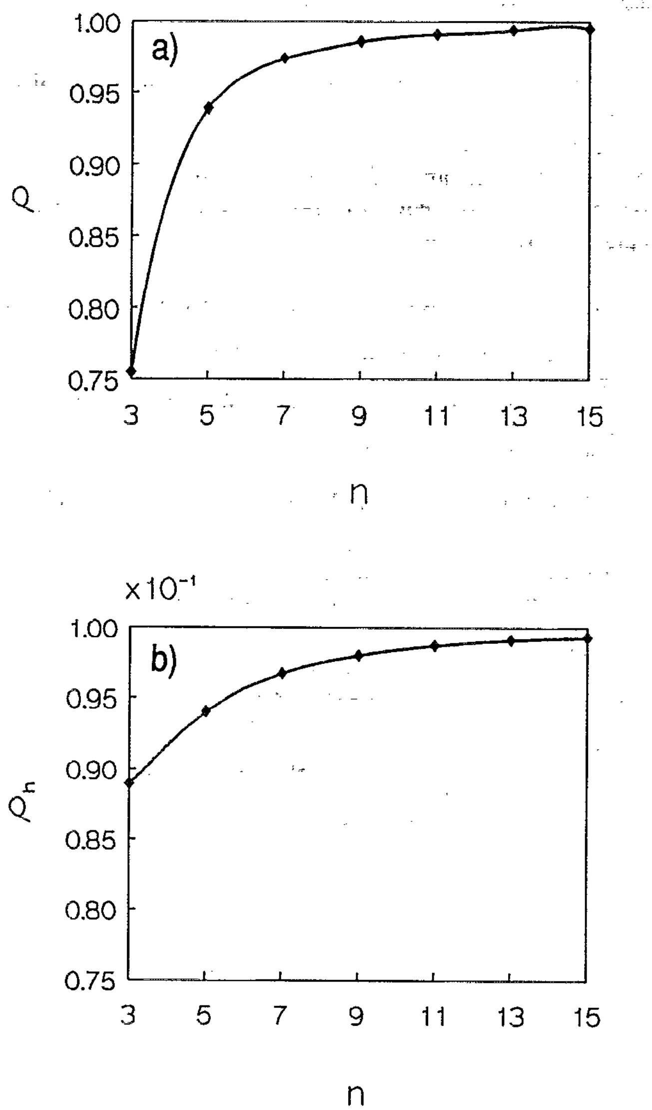

FIG. 16. (a) The calculated resistivity from the Van der Pauw technique as a function of the mesh size n. (b) The calculated Hall resistivity also as a function of n.

the N current densities in the lattice. Solving for $\mathbf{J}$ gives the current density distribution in the film.

Determining *N*

In the 2D case, Eq. (A1) sums the currents to zero at all but one of the nodes which yields a total of $n^2 - 1$ equations. Equation (A2) sums the electric field around each loop in a given tile and sets the result to zero. This process is applied to all the tiles leading to $(n - 1)^2$ equations. Hence the total number of equations in the 2D case is $2\times n\times(n-1)$. In the 3D lattice, Eq. (A1) has to account for the upper and lower lattice, hence $2 \times n^2 - 1$ equations are obtained. Equation (A2) is applied to all the tiles except the ones in the upper layer of the lattice leading to $(n - 1)^2 + 2 \times n \times (n - 1)$ equations. Hence the total number of equations in the 3D case is $n\times(5n-4)$ equations.

Determining *n*

The nodes covering the sample can be thought of as sampling points. A larger n implies a higher current resolution on the sample. In order to determine an appropriate value for n, a Van der Pauw[13] resistivity calculation is presented on the 2D lattice. The Van der Pauw computation of the resistivity consists of connecting four wires at the circumference of a sample of arbitrary shape. Let A, B C, and D, be four successive contacts fixed on the periphery of a square sample as shown in Fig. 15. We apply a current density J_0 through contacts A and B and calculate the potential difference between contacts C and D (V_{CD}). We define $R_{CD,AB}$ as the resistance of the film by dividing V_{CD} by the current flowing across A and B,

$$R_{CD,AB} = V_{CD} / J_0\, tl. \tag{A6}$$

The potential difference V_{CD} is obtained by adding up the electric field along an arbitrary path,

$$V_{CD} = \sum_{\substack{\text{links on a} \\ \text{path from C to D}}} El. \tag{A7}$$

As shown in Fig. 15, A, B, C, and D are located symmetrically at the edge of the lattice; in this particular case the resistivity of the film is given by[13]

$$\rho_{calc} = \frac{\pi}{\ln 2} R_{CD,AB}\; t = \frac{\pi}{\ln 2} \frac{V_{CD}}{J_0\, l}. \tag{A8}$$

According to Van der Pauw's technique, ρ_{calc} will converge to the intrinsic resistivity of the film when points A, B, C, and D are sufficiently small, i.e., "pointlike" contacts. In other words, the nodes themselves will become sampling points as ρ_{calc} approach the true resistivity of the film.

By setting $\rho_x = \rho_y = 1$ and $\rho_h = 0$ throughout the film, ρ_{calc} is obtained for different 2D mesh sizes n. Figure 15 shows the current density distribution with 49 nodes covering the sample ($n=7$). In this case, $\mathbf{J}_{appl}$ contains two nonzero elements corresponding to an input current density J_0 and an output current density $-J_0$ applied and collected through nodes A and B, respectively. Figure

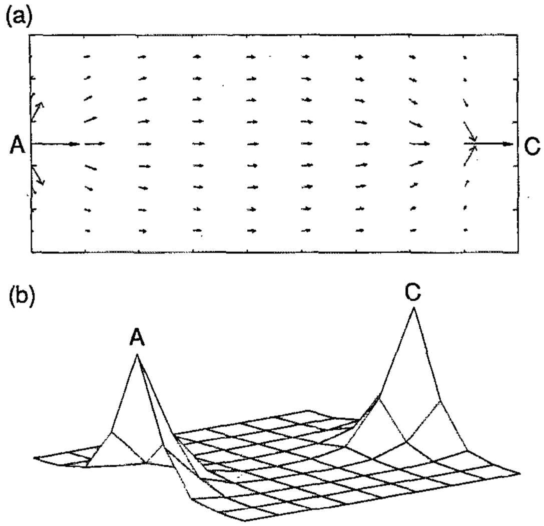

FIG. 17. A 3D current distribution using point contacts A and C: (a) the current distribution in the upper lattice, and (b) the distribution of current in the z direction.

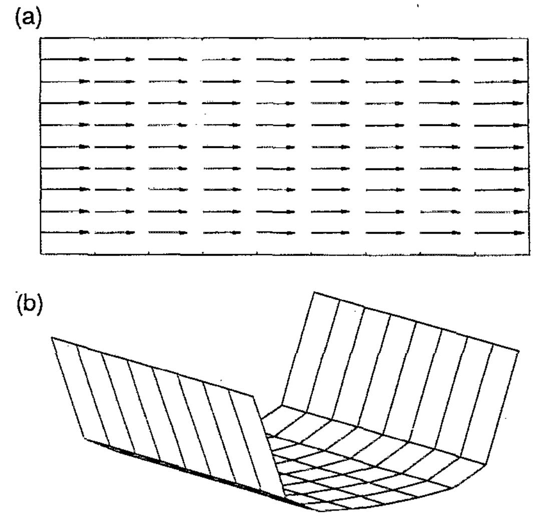

FIG. 18. A 3D current distribution using bar contacts on opposite sides of the sample: (a) the current distribution in the upper lattice, and (b) the distribution of current in the z direction.

16(a) is a plot of ρ_{calc} vs n. For $n=15$, $\rho_{\text{calc}} = 0.995$ which is only 0.5% less than the actual value of ρ. Figure 16(b) displays ρ_h calculated also from the Van der Pauw technique, when the film's ρ_h is set to 0.1 throughout the lattice. In that case the current is applied through points A and C and the voltage is computed across points B and D. ρ_h is then obtained by dividing V_{BD} by I_0 and multiplying it by t.

From Fig. 16(a) we can choose an appropriate mesh size. In this paper we chose the value of $n=15$ for the 2D simulations. In order to reduce the computational time without sacrificing numerical accuracy we choose $n=9$ in the 3D simulations (in this case ρ_{calc} is within 1% of ρ). Figure 17(a) displays the current density distribution in the 3D case in the upper layer of the lattice when the external current density is applied across points A and C. Figure 17(b) is a plot of the current density that flows in the z direction when $t=l$. Figures 18(a) and 18(b) also represent a 3D current density distribution except that now the sample is subjected to a uniform current density applied through one edge and collected through the opposite side (this is known as a bar contact as opposed to the point contact in the previous case). When simulating magneto-optical films we set $l=1$ and $t = 10^{-4}$ and use point contacts since bar contacts are more difficult to achieve experimentally.

Finally, we would like to add that the model presented here can be easily applied to study in-plane magnetic media or to calculate the effects of probe geometry and their location on the sample.

[1] K. Okamoto, T. Shirakawa, S. Matsushita, and Y. Sakurai, AIP Conf. Proc. **18**, 918 (1973).
[2] R. A. Hajjar, M. Mansuripur, and H.-P. D. Shieh, J. Appl. Phys. **69**, 7067 (1991).
[3] S. Yumoto, K. Toki, O. Okada, and H. Gokan, IEEE Trans. Magn. **MAG-24**, 2793 (1988).
[4] R. A. Hajjar, T. Wu, and M. Mansuripur, J. Appl. Phys. **70**, 6041 (1991).
[5] N. F. Mott, Proc. R. Soc. London Ser. A **153**, 699 (1936); **156**, 361 (1936).
[6] I. A. Campbell and A. Fert, *Ferromagnetic Materials,* Vol. 3, edited by E. P. Wohlfarth (Elsevier, Amsterdam, 1982).
[7] D. L. Partin, M. Karnezos, L. C. deMenezes, and L. Berger, J. Appl. Phys. **45**, 1852 (1974).
[8] J. Smit, Physica **17**, 612 (1951).
[9] L. Berger, J. Phys. Chem. Solids **35**, 947 (1974).
[10] L. Berger, J. Appl. Phys. **49**, 2156 (1978).
[11] J. C. DeLuca, R. J. Gambino, and A. P. Malozemoff, IEEE Trans. Magn. **MAG-14**, 500 (1978).
[12] J. C. Deluca, R. J. Gambino, A. P. Malozemoff, and L. Berger, J. Appl. Phys. **52**, 6168 (1981).
[13] L. J. Van der Pauw, Philips Tech. Rev. **20**, 220 (1958).